Applied Surface Science 394 (2017) 509–518

Contents lists available at ScienceDirect

Applied Surface Science

journal homepage: www.elsevier.com/locate/apsusc

Full Length Article

Methanol decomposition on low index and stepped CeO_2 surfaces from GGA+*U*

Walter G. Reimers, María M. Branda*

Departamento de Física e Instituto de Física del Sur, Universidad Nacional del Sur, Bahía Blanca, Av. Alem 1253, 8000, Bahía Blanca, Argentina

ARTICLE INFO

Article history:
Received 27 July 2016
Received in revised form 19 October 2016
Accepted 23 October 2016
Available online 24 October 2016

Keywords:
Catalysis
DFT
Methanol decomposition
Oxide

ABSTRACT

GGA + U calculations have been carried out to study the complete methanol decomposition on the more stable Ceria surfaces, i.e. (111), (221), (331) and (110). These results have shown that the methanol adsorption is exothermic on oxidized as well as on the partially reduced surfaces though the adsorption energy is greater for the latest. The first dehydrogenation step of methanol is highly probable for all the studied sites with activation barriers smaller than 0.2 eV. The first dehydrogenation reaction could also occur by breaking the C—H methyl bond, but we found that this reaction is very unlikely. Reaction and activation energies for the second dehydrogenation – from methoxy to formaldehyde, are very similar for perfect (111) and stepped surfaces but these activation barriers are not negligible, almost ten times as many the first step barriers. Next, the formaldehyde decomposition to formyl and CO species on perfect CeO_2(111) have an important energetic cost, therefore these reactions could occur only on stepped surfaces.

© 2016 Elsevier B.V. All rights reserved.

1. Introduction

Finding alternatives to produce energy with lower emissions of pollutants and higher efficiencies compared to internal combustion is required. The use of proton exchange membrane (PEM) fuel cell system would be an excellent option. PEM fuel cells convert hydrogen gas into useful electric power with a great efficiency, with water as the only by product. However, from a point of view of storage technology and safety topics, hydrogen gas cannot be adequately stored on-board for mobile applications. The reforming of liquid hydrocarbons to produce hydrogen gas has been found as an attractive process to provide the necessary hydrogen for the fuel cell [1]. Methanol is one of the easiest hydrocarbons to reform. Unlike gasoline or diesel fuels, methanol reforming has a couple of advantages. Liquid methanol can be produced by biomass and it is easy to transport and store. It has high hydrogen density; and its decomposition is a simple way to generate hydrogen [1].

Cerium oxide is an important component in many catalytic processes due to its reduction/oxidation ability between the trivalent and tetravalent cerium oxidation states [2,3]. Its peculiar characteristics have been the object of great interest for various heterogeneous catalytic reactions, including several key applications in solid oxide fuel cells [4,5].

More than few works of methanol decomposition using catalysts supported on Ceria surfaces have been carried out; Brown et al. [6] found that Pt/ceria-alumina catalysts are very selective and active for this reaction and Ceria promoted catalysts are significantly more active than unpromoted catalysts. By means of TEM, ESCA, and XAFS analyses, Imamura et al. [7] studied methanol decomposition on supported precious metals- by performing a kinetic analysis, and they also showed that ceria was the best support. Methanol adsorption and reaction have been studied on Rh-deposited cerium oxide thin films under UHV conditions using TPD and synchrotron soft X-RPS. Methanol adsorbed on the ceria films deprotonating to form methoxy as the only intermediate on the surface. This methoxy is decomposed and desorbed as CO and H_2 at higher temperatures regardless of the ceria oxidation state; the reduced ceria can promote total methanol decomposition on Rh. [8] Mullins et al. [9] through TPD, O 1 s XPS and C k-edge NEXAFS measurements found that the main reaction products obtained by methanol on oxidized CeO_2 films – deposited on Ru(0001)- are H_2O at low temperatures and CH_2O at high temperatures. On the other hand, on reduced Ceria more methanol can be adsorbed and it undergoes more extensive decomposition producing CO and H_2 near 640 K, in addition to formaldehyde and water. As the degree of ceria reduction increases, more H_2 and less H_2O are produced. Methanol does not require surface oxygen vacancies to chemisorb and it is a good reductant for ordered Ceria films. The same authors [10] observed the presence of alkoxy and hydroxyl species after the adsorption of methanol, ethanol and propanol on surfaces of

* corresponding author.
E-mail address: cabranda@criba.edu.ar (M.M. Branda).

http://dx.doi.org/10.1016/j.apsusc.2016.10.154
0169-4332/© 2016 Elsevier B.V. All rights reserved.

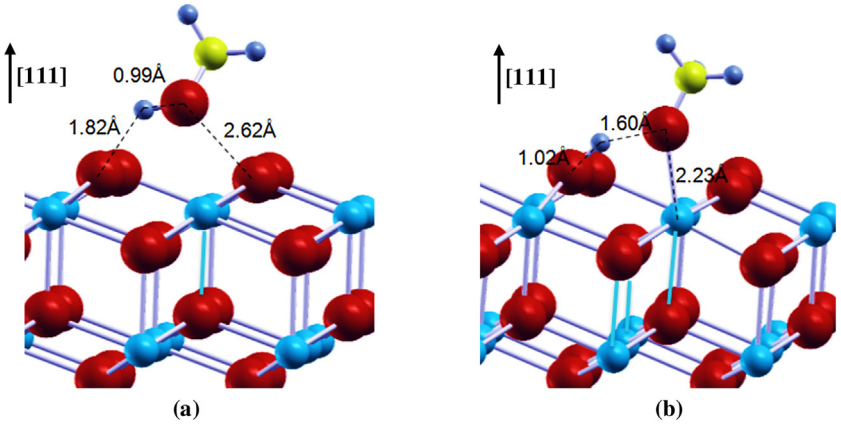

Fig. 1. (a) Methanol adsorption on $CeO_2(111)$ surface. IS of **STEP a**$_1$. (b) Methoxi + H co-adsorption on $CeO_2(111)$ surface. FS of **STEP a**$_1$. Blue spheres correspond to Ce atoms, red: O atoms, yellow: C atom and grey: H atoms. (For interpretation of the references to colour in this figure legend, the reader is referred to the web version of this article.)

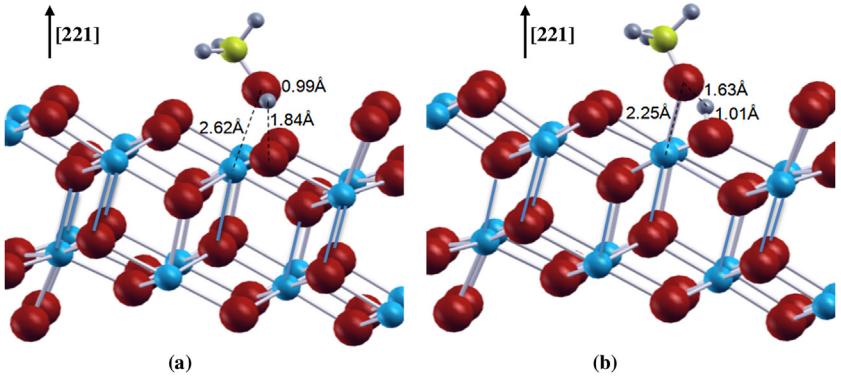

Fig. 2. (a) Methanol adsorption on $CeO_2(221)_I$ surface site. IS of **STEP a**$_1$. (b) Methoxi + H co-adsorption on $CeO_2(221)_I$ surface site. FS of **STEP a**$_1$. Blue spheres correspond to Ce atoms, red: O atoms, yellow: C atom and grey: H atoms. (For interpretation of the references to colour in this figure legend, the reader is referred to the web version of this article.)

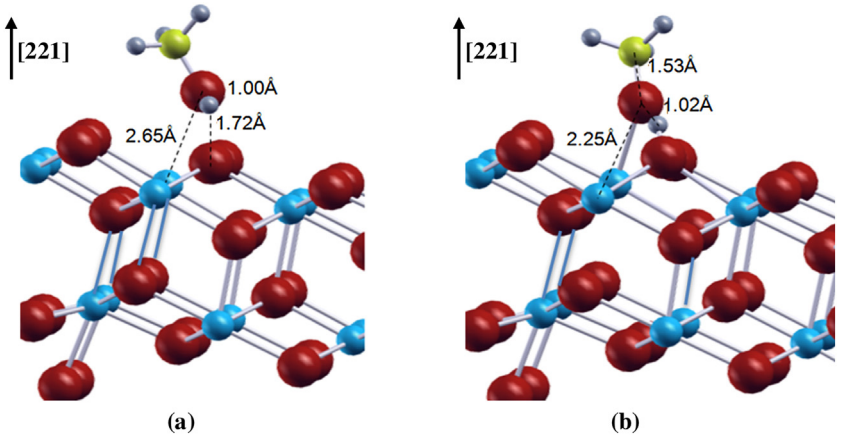

Fig. 3. (a) Methanol adsorption on $CeO_2(221)_M$ surface site. IS of **STEP a**$_1$. (b) Methoxi + H co-adsorption on $CeO_2(221)_M$ surface site. FS of **STEP a**$_1$. Blue spheres correspond to Ce atoms, red: O atoms, yellow: C atom and grey: H atoms. (For interpretation of the references to colour in this figure legend, the reader is referred to the web version of this article.)

$CeO_2(111)$. They found that primary alcohols favor dehydrogenation products such as aldehydes and reduce ceria due to the loos of oxygens. On pure ceria, CH_3OH dissociates to produce CH_3O and OH on both oxidized and reduced surfaces by 200 K. The CH_3O reacts with oxidized ceria to produce formaldehyde at elevated temperatures. Although formaldehyde is also produced on a reduced ceria surface, methoxy primarily decomposes to CO and H_2 [10].

XPS, LEED, TPD and FT-RAIRS measurements have been carried out to study the adsorption of methanol on ordered epitaxial layers of cerium oxides grown on a Cu(111). The decomposition temperature of the methoxy groups is slightly lower at sites near the edges of the oxide islands than on the (111) surface of thicker oxide films, and the copper surface itself can mediate the decomposition processes at very low oxide coverages [11].

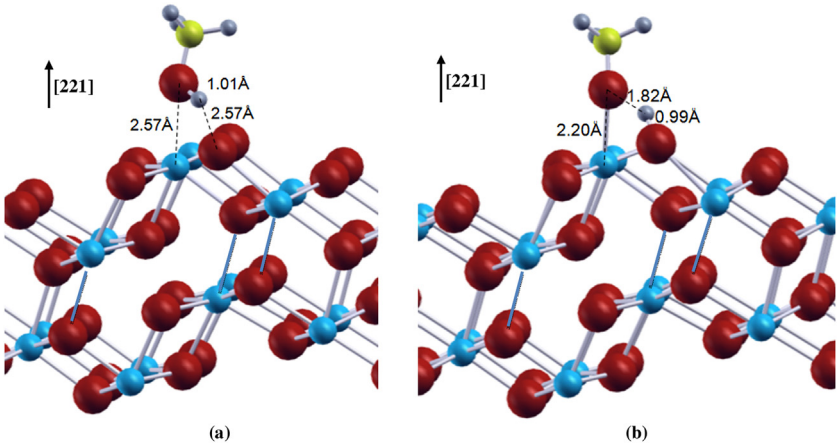

Fig. 4. (a) Methanol adsorption on $CeO_2(221)_T$ surface site. IS of **STEP a**$_1$. (b) Methoxi + H co-adsorption on $CeO_2(221)_T$ surface site. FS of **STEP a**$_1$. Blue spheres correspond to Ce atoms, red: O atoms, yellow: C atom and grey: H atoms. (For interpretation of the references to colour in this figure legend, the reader is referred to the web version of this article.)

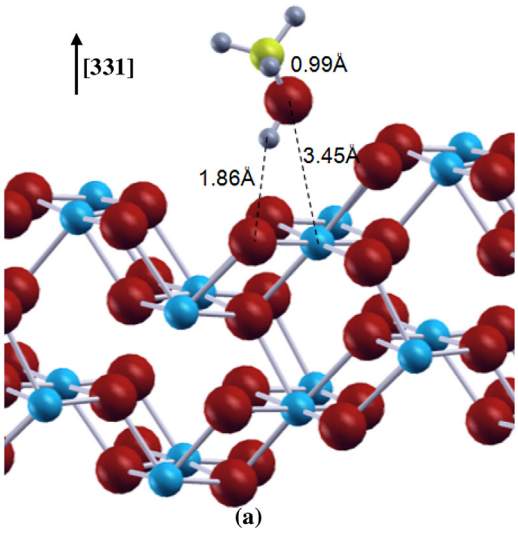

Fig. 5. (a) Methanol adsorption on $CeO_2(331)_I$ surface site. IS of **STEP a**$_1$. Blue spheres correspond to Ce atoms, red: O atoms, yellow: C atom and grey: H atoms. (For interpretation of the references to colour in this figure legend, the reader is referred to the web version of this article.)

IR, Raman and mass spectroscopy studies on ceria nanocrystals – containing (110), (100) and (111) faces- have shown methoxy species adsorbed on mono, di and tri-coordinated sites for (110) and (100) faces but only methoxy on Top for the (111) face [12].

Mei et al. [13,14] studied by Density Functional Theory (DFT) the methanol adsorption on $CeO_2(111)$ and (110) surfaces. They found that methanol can absorb on the surface either molecularly or dissociatively. For these authors, at 0.25 ML coverage, the most stable structure for methanol adsorption is the dissociative adsorption forming both $-OCH_3$ + H and $HOCH_2$ by O—H and C—H bond breaking, respectively. They found that the most stable molecularly adsorbed structure occurs with adsorption energies of 0.48 eV on $CeO_2(111)$ and 0.59 eV on $CeO_2(110)$. The thermodynamic stability order on the (110) surface at 0.25 ML is the same as the one on the (111) surface: C—H bond scission > O—H bond scission > C—O bond scission.

Beste et al. [15], from PW91 + U calculations, have studied the methanol adsorption on oxidized and partially reduced $CeO_2(111)$. They found no qualitative effect of spin state but the adsorption energies are influenced by the introduction of the Hubbard (U) term. Methanol adsorption is exothermic on oxidized and partially reduced surfaces. These authors [16] have also examined the effect of coadsorbates on the dissociation of methanol on $CeO_2(111)$. The inclusion of coadsorbed H is necessary to diminish the C—H scission barrier. More recently [17], they have analyzed the Temperature-Programmed Desorption (TPD) of $CeO_2(111)$ surface with high coverage of methanol and explained the low-temperature water formation and high-temperature methanol desorption.

Kropp et al. [18], also using DFT + U calculations and periodic models, have studied the adsorption and dissociation of methanol on species of monomeric vanadia supported on the $CeO_2(111)$ surface. They found that the methanol adsorption is highly exothermic with adsorption energies of 1.8 to 1.9 eV. The same authors [19] have also studied methanol adsorption and dehydrogenation at the perfect $CeO_2(111)$ and O-defective surfaces. They compared PBE, PW91 (GGA) and hybrid calculations using dispersion and van der Waals corrections; they found a good agreement between PBE + U + D and HSE + D results. The dissociative adsorption values from PW91 and PBE + U approaches on the perfect $CeO_2(111)$ were 0.84 and 0.69 eV, respectively. More recently [20], they carried out calculations for converting methanol to formaldehyde on the pristine and defective surfaces of $CeO_2(111)$ and on pristine $CeO_2(100)$. They found that, for $CeO_2(111)$, hybrid functionals tend to be in better agreement with experiment and that the defective surface has a higher barrier for C—H scission to formaldehyde than the pristine surface (1.34 and 1.25 eV, respectively).

The influence of exposed surfaces in nanostructures of cerium oxide to produce formaldehyde or CO + H from the decomposition of methanol was recently studied. From PBE calculations describing how different surfaces lead to the decomposition of formaldehyde or CO + H. The authors conclude on the importance of controlling the way of catalytic processes [21].

More recently, the CO_2 reduction to methanol on extended $CeO_2(110)$, reduced and non-reduced surfaces, was investigated from DFT calculations by Kumari et al. [22,23]. They found that from a RWGS mechanism a carboxyl group produces CO, and then, it is hydrogenated to produce methanol.

On the other hand, Chen et al. have studied the CO_2 activation and dissociation on ceria (110) surface [24] and later, the conversion to methanol by hydrogenation of CO_2 on reduced ceria (110) from DFT + U calculations [25]. They show that CO_2 hydro-

Table 1
Relevant structural data and adsorption energy (E_{ads}) of CH_3OH on the ceria (111), (221), (331) and (110) surfaces.

Surface	d_{O-Ce} (Å)	d_{O-H} (Å)	$d_{Osurf-H}$ (Å)	∠HOC (°)	E_{ads} (eV)
(111)	2.62	0.99	1.82	114.6	−0.49 (−0.52)
$(221)_I$	2.62	0.99	1.84	113.8	−0.46 (−0.56)
$(221)_M$	2.65	1.00	1.72	113.1	−0.42
$(221)_T$	2.57	1.01	1.67	113.5	−0.66
$(331)_I$	3.45	0.99	1.86	111.6	−0.19
$(331)_M$	2.59	1.01	1.72	114.5	−0.71 (−0.72)
$(331)_T$	2.57	1.03	1.61	112.2	−0.71
(110)	2.62	1.02	1.65	113.0	−0.64

Molecular adsorption on I: internal surface oxygen, M: middle surface oxygen and T: top surface oxygen.
E_{ads} (H_2O) between brackets [45].
Free methanol: d_{O-H} (Å) = 0.97, ∠ HOC (°) = 108.4

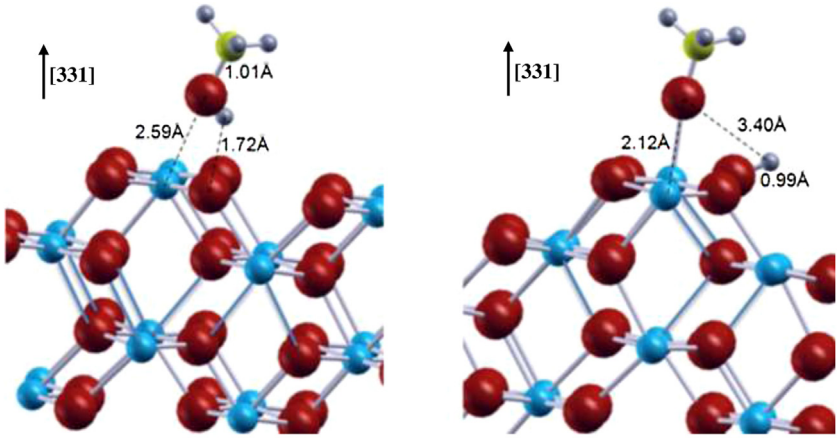

Fig. 6. (a) Methanol adsorption $CeO_2(331)_M$ surface site. IS of **STEP a**$_1$. (b) Methoxi + H co-adsorption on $CeO_2(331)_M$ surface site. FS of **STEP a**$_1$. Blue spheres correspond to Ce atoms, red: O atoms, yellow: C atom and grey: H atoms. (For interpretation of the references to colour in this figure legend, the reader is referred to the web version of this article.)

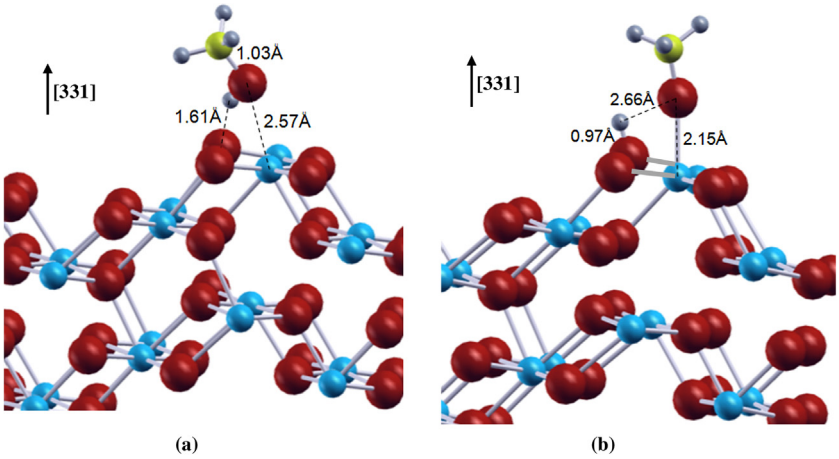

Fig. 7. (a) Methanol adsorption on $CeO_2(331)_T$ surface site. IS of **STEP a**$_1$. (b) Methoxi + H co-adsorption on $CeO_2(331)_T$ surface site. FS of **STEP a**$_1$. Blue spheres correspond to Ce atoms, red: O atoms, yellow: C atom and grey: H atoms. (For interpretation of the references to colour in this figure legend, the reader is referred to the web version of this article.)

genation to methanol on this catalyst should predominantly follow the formate pathway. In this pathway, H-formalin is converted to formaldehyde in the rate-limiting step, followed by further hydrogenation to form a surface-bound methoxy group and finally, methanol.

Although the study of methanol decomposition has been carried out by several authors, these reactions on stepped surfaces were not

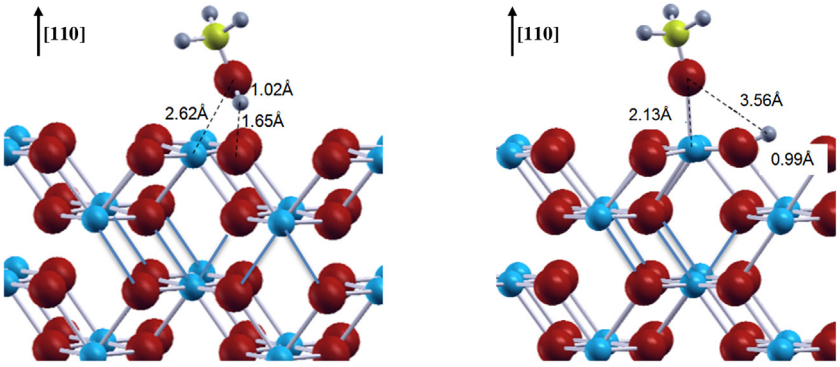

(a) (b)

Fig. 8. (a) Methanol adsorption on CeO_2(110) surface. IS of **STEP a$_1$**. (b) Methoxi + H co-adsorption on CeO_2(110) surface. FS of **STEP a$_1$**. Blue spheres correspond to Ce atoms, red: O atoms, yellow: C atom and grey: H atoms. (For interpretation of the references to colour in this figure legend, the reader is referred to the web version of this article.)

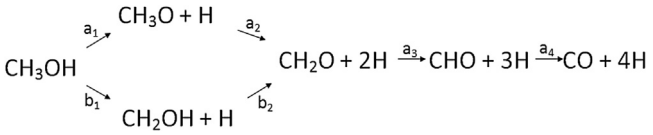

Fig. 9. Stepwise of methanol dehydrogenation reactions.

Table 2
Activation (E_{act}) and reaction (E_{reac}) energies (in eV) for methanol dissociation –**STEP a$_1$**- on (111), (221), (331) and (110) ceria surfaces.

Surface	E_{act}	$E^{-1}{}_{act}$	E_{reac}
(111)	+0.18	+0.13	+0.05
	(+0.19)	(+0.05)	(+0.14)
$(221)_I$	+0.19	+0.06	+0.13
	(+0.31)	(+0.04)	(+0.27)
$(221)_M$	+0.18	+0.06	+0.12
$(221)_T$	+0.03	+0.15	−0.12
$(331)_M$	+0.21	+0.51	−0.30
	(+0.21)	(+0.35)	(−0.14)
$(331)_T$	+0.21	+0.34	−0.13
(110)	+0.09	+0.61	−0.52

$(331)_I$ adsorption site was not analyzed because of the improbable methanol adsorption in this place (see de E_{ads} in Table 1).
Data between brackets correspond to H_2O dissociation [45].

Table 3
Activation (E_{act}) and reaction (E_{reac}) energies (in eV) for **STEP a$_1$**, **STEP b$_1$**, **STEP a$_2$**, **STEP a$_3$** and **STEP a$_4$** on (111) and, $(331)_M$ ceria surface sites.

	Surface	E_{act}	E_{reac}
STEP a$_1$	(111)	+0.18	+0.05
	$(331)_M$	+0.21	−0.30
STEP b$_1$	(111)	+4.43	−0.61
	$(331)_M$	+1.37	+1.07
STEP a$_2$	(111)	+1.65	−0.50
	$(331)_M$	+1.78	−0.58
STEP a$_3$	(111)	+3.20	+0.23
	$(331)_M$	+1.31	+0.02
STEP a$_4$	(111)	+1.73	+1.59
	$(331)_M$	+1.48	+1.31

been analyzed yet. In the present work, we analyze and compare the methanol decomposition on the more stable surfaces of Ceria [26] i.e. (111), (221), (331) and (110), using GGA + U calculations.

2. Computational details

Methanol adsorption and decomposition on different sites of the (111), (221), (331) and (110) low index Miller ceria surfaces have been studied by means of periodic density functional theory (DFT) calculations with repeated slab model. These calculations have been carried out using the PW91 [27,28] form of the Generalized Gradient Approximation (GGA) corrected with the so called on-site Hubbard parameter (*U*) [29]. GGA averages the exchange correlation of the electronic interaction, but does not correct the non-physical interaction of electrons derived from classical Coulomb repulsion interelectronic. When studying the CeO_{2-x} with reduced Ce atoms, the Ce-4f strongly localized band is partially occupied and therefore GGA describes poorly the electronic structure. The difficulties of GGA can be overcome making use of more sophisticated forms for the exchange correlation potential. The *U* value was chosen taking into account the experience obtained from previous works [30–35], specifically in this one we use U_{eff} = 4 eV. A plane wave basis set with 415 eV cut-off energy was enough to represent the valence density allowing a convergence up to 10^{-4} eV in the total energy while the projector augmented-wave method (PAW) [36] was used to describe the atomic cores. A Monkhorst–Pack grid [37] with k-point samplings were considered for every case and it was of at least (5 × 5 × 1). The Methfessel-Paxton smearing of width σ = 0.05 eV was applied and the reported total energies were then extrapolated to σ → 0 eV [38].

In order to ascertain the contribution by dispersion, additional calculations were performed with DFT-D and compared to the DFT results. Methanol adsorption on the (111) and $(331)_M$ sites were calculated taking into account dispersion effects; these calculations were carried out using an empirical correction to comprise dispersion forces, as suggested by Grimme [39] and indicated by *disp* for simplicity:

$$E^{DFT-D} = E^{DFT} + E^{disp}$$

where E^{DFT-D} is the total energy of the system, E^{DFT} is the Kohn-Sham total energy as obtained from pure PBE and E^{disp} is an empirical dispersion correction.

The E_{ads} found for (111) surface with and without dispersion were −0.56 eV and −0.51 eV, respectively. On the other hand, the E_{ads} calculated for (331) surface with and without dispersion were −0.70 eV and −0.68 eV, respectively. From these results, we can conclude that dispersion effect on the adsorption energy values is negligible. The slight differences on the E_{ads}, ~0.02 eV, with respect to the values reported on Table 1 are due to the different functionals (PBE[40] and PW91[27,28]). Cheng et al. in their manuscript about hydrogenation of CO_2 on Ceria(110) also have reported that the dispersive forces play only a small role [25].

The influence of zero-point vibrational energy (ZPE) contributions was analyzed. The ZPE for adsorbed CH_3OH, CH_3O, CH_2O, CHO and CO species and for the transition state (TS) energies was

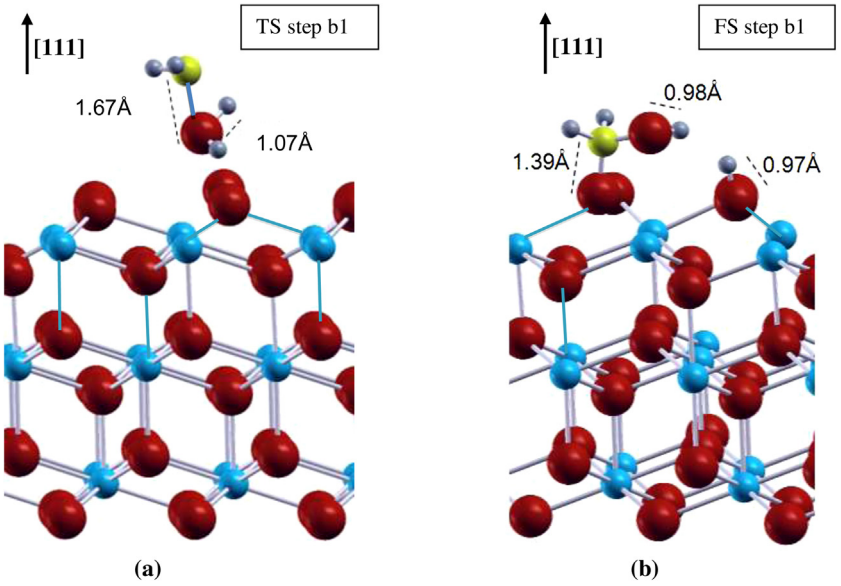

Fig. 10. Geometrical structure corresponding to the (a) TS and (b) FS of **STEP b**$_1$ on (111) surface. Blue spheres correspond to: Ce atoms, red: O atoms, yellow: C atom and grey: H atoms. (For interpretation of the references to colour in this figure legend, the reader is referred to the web version of this article.)

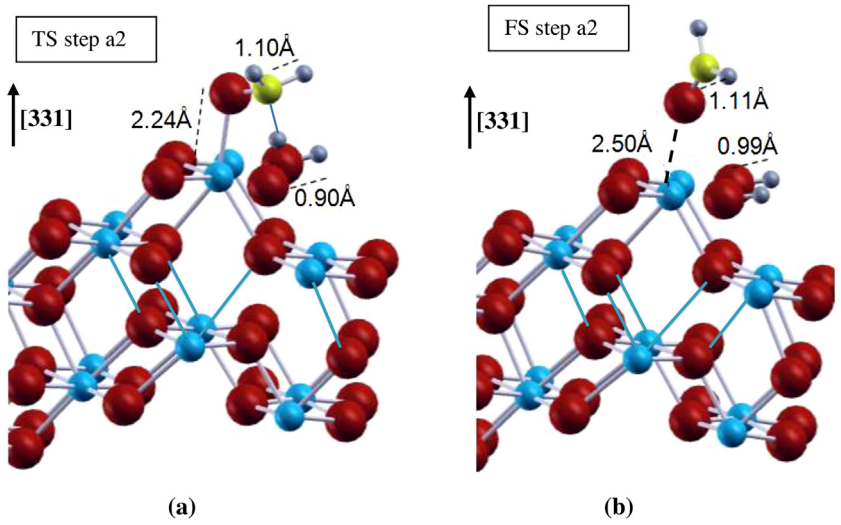

Fig. 11. Geometrical structure corresponding to the (a) TS and (b) FS of STEP a_2 on $(331)_M$ surface site. Blue spheres correspond to: Ce atoms, red: O atoms, yellow: C atom and grey: H atoms. (For interpretation of the references to colour in this figure legend, the reader is referred to the web version of this article.)

analyzed and the differences found were negligible (lower than 0.005 eV). For this reason, it was possible to neglect this correction in our results.

Climbing-image Nudged Elastic Band method (CI-NEB) [41] was used to obtain the transition states (TS) for each step of the methanol dissociation. The energy minimal states and transition states were confirmed carried out frequency calculations. The initial and final states were verified with all values of real vibrational frequencies. On the other hand, the transition states were confirmed by obtaining a single imaginary frequency corresponding to the reaction mode. Adsorption energies were calculated from:

E_{ads} = E(Methanol/surface) – E(Methanol) – E(surface);

activation barriers as:

E_{act} = E(TS) – E(IS);

and the reaction energies as:

E_{reac} = E(FS) – E(IS);

where E(Methanol/surface) is the total electronic energy of methanol adsorbed on a surface, E(Methanol) is the total energy of the free molecule, E(surface) is the total energy of the surface slab; E(IS), E(TS) and E(FS) are the total energies of the initial, transition and final states, respectively.

All the calculations were performed at the spin-polarized level and it have been carried out with the *Vienna Ab-Initio Simulation Package* (VASP) [42,43].

3. Surface models

The study of methanol decomposition on ceria surfaces with periodic density functional calculations as described in the previous section has been done for (111), (110), (221) and (331) slab models built from the CeO_2 bulk cubic (Fm3m) CaF_2 structure. These surfaces have shown to be the most stable ones from energetic point of view [26]. A sufficiently wide vacuum width between

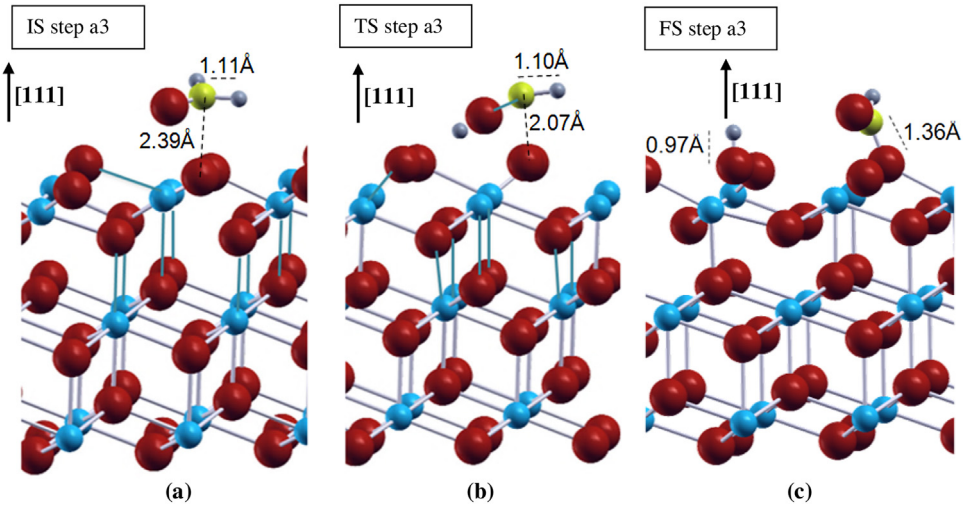

Fig. 12. Geometrical structure corresponding to the (a) IS, (b) TS and (c) FS of **STEP a$_3$** on (111) surface. Blue spheres correspond to: Ce atoms, red: O atoms, yellow: C atom and grey: H atoms. (For interpretation of the references to colour in this figure legend, the reader is referred to the web version of this article.)

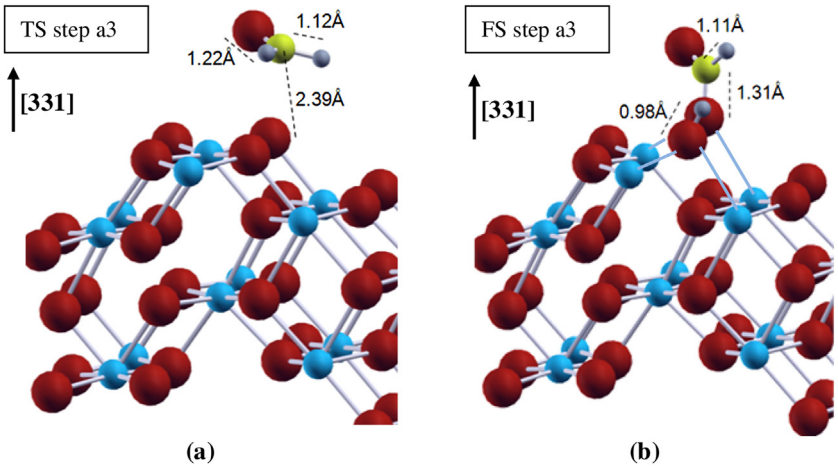

Fig. 13. Geometrical structure corresponding to the (a) TS and (b) FS of **STEP a$_3$** on (331) surface. Blue spheres correspond to: Ce atoms, red: O atoms, yellow: C atom and grey: H atoms. (For interpretation of the references to colour in this figure legend, the reader is referred to the web version of this article.)

the repeated slabs – more than 10Å – was required to avoid the interaction between the adsorbed species and the following slab.

The 2 × 2 (111) slab was built by 3 CeO_2 layers (9 atomic layers), 2 × 2 (110) slab by 4 CeO_2 layers (4 atomic layers), 1 × 2 (221) slab by 8 CeO_2 layers (18 atomic layers) and 1 × 2 (331) slab by 6 CeO_2 layers (18 atomic layers). (111) and (110) surfaces present only one possible site to the adsorption and decomposition of methanol molecule, however, on the stepped (221) and (331) surfaces there are three possible sites- Internal, Medium and Top, named from this point forward: I, M and T respectively.

The slab model selected for (221) and (331) surfaces, with 1 × 2 supercell size, was analyzed in order to avoid possible interactions between the periodic images of the adsorbed molecules. The minimum distances between neighboring molecules of adsorbed methanol are, at the first and the second direction of (221), ~11.5 Å and ~7.7 Å, respectively. The corresponding intermolecular distances for (331) surface are ~8.5 Å and ~7.6 Å, respectively. In addition, the minimum distances between the fragments (methoxy and H) after the first dehydrogenation are ~6.0 Å, ~6.1 Å and ~5.9 Å for (221), (331) and (111) surfaces, respectively. Being all these values greater than 5 Å, we considered that the selected slab sizes are sufficient to avoid spurious interactions due to the periodic images of the molecules and the fragments.

The geometries of adsorbed species – methanol and dissociated methanol, and also the topmost of the substrate, were full optimized by using GGA + U (U = 4 eV) with the experimental lattice parameter value: a_0 = 5.41 Å [44]. The convergence criterion for structural optimization was set to be a total force difference less than 10^{-3} eV for consecutive geometries.

4. Results and discussion

Initially, we have analyzed the methanol adsorption on all possible sites of the CeO_2 surfaces mentioned above. The optimized geometries for every configuration are displayed on Figs. 1(a)–8(a). Favorable (exothermic) adsorption corresponds to negative adsorption energy. We found that the higher adsorption energies (~ −0.7 eV) involve on top (T) sites of the stepped (221) and (331) surfaces; and it is also favorable on the only (110) adsorption site and in the middle (M) of the (331) step (see E_{ads} values on Table 1). These adsorption energies agree with the corresponding values found by Fuente et al. [45] for water on ceria surfaces – see values between brackets. Here it was found again that the adsorption of a molecule containing an OH group is bonded more strongly with surfaces containing lower coordination Ce atoms. Similar results relative to the geometrical structure of adsorbed methanol

and methoxy species on Ceria(110) were found by Kumari et al. [22], although they calculated an adsorption energy slightly greater than the one calculated here. The stronger interactions on these sites are in accord with an increase of the methanol O—H bond length with respect to the free molecule –between 0.04 to 0.06 Å. This increase in bond length would be associated with a charge transfer from the substrate to the σ^* antibond orbital. Hydrogen bond with the surface, d(O_{surf}—H), and d(O_{Meth}—Ce) are close to ~1.7 Å and ~2.6–2.8 Å, respectively (see data on Table 1). In addition, the ∠ HOC angle increases from ~108° to ~113°–115° for all the adsorption sites. In the case of $(331)_I$ site the smaller adsorption energy agrees with the longer Ce-O distance and smaller ∠HOC angle, nearest the free molecule one. Particularly, Mei et al. found similar methanol adsorption energy values of 0.48 eV on $CeO_2(111)$ and 0.59 eV on $CeO_2(110)$ [13,14].

After the adsorption analysis, we have proceeded to study the stepwise of methanol dehydrogenation reactions. Each methanol decomposition step is shown in Fig. 9.

The first dehydrogenation –**STEP a**$_1$, was analyzed starting from the same sites studied for the molecule adsorption – except for the innermost site on (331) surface, where methanol adsorption is very unlikely. The structures corresponding to the final state (FS) of **STEP a**$_1$ are displayed in Figs. 1(b)–8(b). There can be observed methoxy species on top sites, where the methoxy oxygen binds to a second layer cerium atom. This agrees with the results found by Beste et.al.,[15] on the fully oxidized surface.

Activation (E_{act}), reverse activation ($E^{-1}{}_{act}$) and reaction (E_{reac}) energies (in eV) for this step are shown on Table 2. **STEP a**$_1$ reaction is favored on $(221)_T$ and (110) surface sites with activation energies (E_{act}) smaller than 0.10 eV. This barrier is also small and around 0.20 eV for the other sites. The energy barriers for the first dehydrogenation are in the same order than the calculated by Sutton et. al [17]. They found activation barriers between ~0.1 eV and ~0.4 eV on a (111) surface completely covered by methanol molecules.

In addition, the reverse activation energies are, both on (110) as on $(331)_M$ sites, greater than 0.5 eV (see Table 2). Taking into account smaller values of direct barriers and greater reverse barriers we can expect that the reaction shifts towards the dissociated species. The same reactivity had previously been found for water dissociation –(110) and stepped surfaces being more reactive than the (111) one [45]. Besides, TPD, O 1 s XPS and C k-edge NEXAFS measurements [9], have shown that more methanol can be adsorbed on reduced ceria surfaces and it undergoes more extensive decomposition.

Taking into account both the relative stability order of the CeO_2 surfaces [26] and the reactivity order for the first methanol dehydrogenation found for the different sites, we decided to continue the study of the methoxy decomposition only on (111) and $(331)_M$ surface sites. The first surface was selected since it is the most stable ceria surface and $(331)_M$ has shown to be the most reactive site for the methanol adsorption and also for the first dehydrogenation (see the E_{ads} and E_{reac} values in Tables 1 and 2 respectively). Therefore, the following decomposition steps –**STEP a**$_2$ to **STEP a**$_4$, were studied on (111) and $(331)_M$ surface sites.

Before proceeding with the dehydrogenation reaction pathway following a_n steps we believed necessary to study a possible dehydrogenation of the methyl group, breaking a C—H bond –**STEP b**$_1$. Activation (E_{act}) and reaction (E_{reac}) energies for **STEP** to **a**$_4$, and **STEP b**$_1$ on (111) and, $(331)_M$ ceria surface sites are displayed on Table 3. Here we can see that the C—H bond breaking is so much unlikely than the O—H one (**STEP a**$_1$). Although the E_{reac} for (111) surface is endothermic, its energy barrier is very high – almost 5 eV. On the other hand, breaking this bond on the (331) surface requires an activation energy of ~1.4 eV and a reaction energy of ~1 eV. The structure corresponding to the TS and FS of **STEP b**$_1$ on (111) site are displayed in Fig. 10(a) and (b) respectively. The distance between

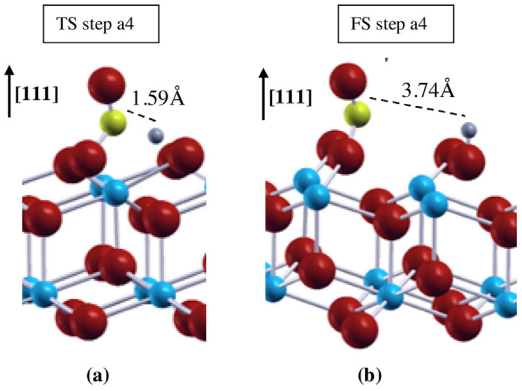

Fig. 14. Geometrical structure corresponding to the (a) TS and (b) FS of **STEP a**$_4$ on (111) surface. Blue spheres correspond to: Ce atoms, red: O atoms, yellow: C atom and grey: H atoms. (For interpretation of the references to colour in this figure legend, the reader is referred to the web version of this article.)

the broken H and the C atom is > 3.5 Å (not shown) at the FS. The geometry found for the transition state (TS) was very different to the IS (see Fig. 1a) and FS ones; this would explain the great energy barrier of this reaction. Therefore, taking into account that the first dehydrogenation will be much more favorable through **STEP a**$_1$ than **STEP b**$_1$, we decided that **STEP b**$_2$ is not necessary to evaluate.

Methoxy dehydrogenation leads to formaldehyde, **STEP a**$_2$. The reaction and activation energies for the second dehydrogenation – from CH_3O to CH_2O, are very similar for both selected sites (see Table 3). As it can be observed, the E_{reac} are noticeably endothermic but the activation barriers are not negligible – between 1.6 and 1.9 eV, almost ten times as many **STEP a**$_1$ barriers. These values also agree with the ones calculated by Sutton et al. who obtained energy barriers between 1.1 and 1.2 eV for completely covered (111) surfaces [17]. These significant energy barriers could be attributed to the geometric change observed from the initial state (IS) to the transition state (TS) of **STEP a**$_2$; see Figs 6(b) and 11 (a), respectively. On the other hand, Fig. 11(b) shows the final geometry of this step also on the $(331)_M$ site.

Once again, in the third step of the dehydrogenation –**STEP a**$_3$, it was found that the stepped (331) surface is more reactive than the (111) surface. Although the reaction energy values are small for both surface sites, the activation energies are not negligible, specially the calculated for (111) surface (> 3 eV). As shown in Fig. 12(a) and (b) there is an important geometric change from the IS to the TS on (111) surface, however this change is not so pronounced on the $(331)_M$ site (see Fig. 13(a)). Finally, the FS on the sites (111) and $(331)_M$ are very similar (see Figs. Fig. 1212(c) and Fig. 1313(b) respectively).

The last step which leads to the complete dehydrogenation until CO –**STEP a**$_4$, shows similar reactivities on both (111) and (331)M surface sites, but with slightly smaller values of activation and reaction energies for the stepped $(331)_M$ site. The reaction energies of this last step are large and close to the activation ones. Thus, the reverse activation energies are small and this fact is correlated with very similar geometries between the TS and FS (see Fig. 14(a) and (b) respectively).

In order to do a more complete analysis about these reactions, all the reaction steps were described on Fig. 15a–b. The reference value of energy equal to zero corresponds to $E(Methanol)_{gas}$ + E(pristine surface) for both figures. At a glance, it can be observed that all the TS and the FS energies for (111) surface are higher than the ones for (331). From the adsorbed methanol molecule on the (111) surface it can be appreciated that **STEP a**$_1$ is much more favored than **STEP b**$_1$ and also more than the desorption reaction (see Fig. 15a). Subsequently, **STEP a**$_2$, from methoxy towards formaldehide, is

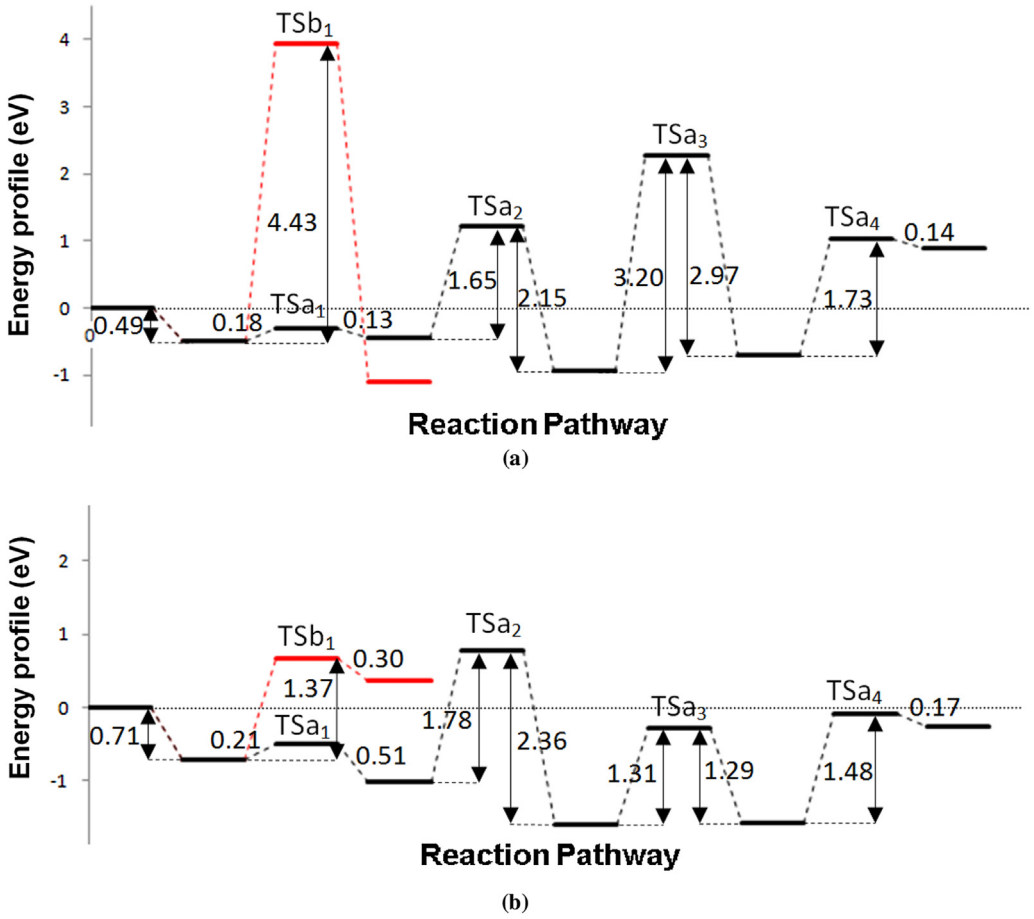

Fig. 15. Energy profiles (eV) for all the reaction steps: (a) on (111) surface (b) on $(331)_M$ surface site. The reference value of energy equal to zero corresponds to $E(Methanol)_{gas} + E(pristine\ surface)$.

more difficult than the first because of the activation reaction about ~1.6 eV. This fact agrees with XPS, LEED, TPD and FT-RAIRS results, whose measurements show that CH_3O reacts with oxidized ceria to produce formaldehyde at elevated temperatures [10]. After the second step of dehydrogenation, this surface would not be reactive to produce neither formyl nor CO due to the large energy barrier found for **STEP** $\mathbf{a}_3$. In addition, the reverse reaction from formaldehyde to methoxy is also difficult. Then, either adsorbed methoxy or adsorbed methanol are both the most probable and stable species on this surface. Then, the stability of the adsorbed species on (111) follows this order: $CH_2O > CHO > CH_3O \sim CH_3OH$.

On the other hand, **STEP** $\mathbf{a}_1$ is more favored than **STEP** $\mathbf{b}_1$ on $(331)_M$ sites; and also more than the desorption reaction (see Fig. 15b). The second dehydrogenation reaction towards formaldehyde is also difficult on this surface, even more than **STEP** $\mathbf{b}_1$. However, the TSa_3 and TSa_4 relative energies for this stepped surface are much smaller than the energies for the (111) surface, showing thus to be a more reactive surface. The stability of the adsorbed species on $(331)_M$ follows this order: $CH_2O \sim CHO > CH_3O > CH_3OH$.

5. Conclusions

To summarize, the methanol adsorption can take place on all surfaces studied in this work with energies between ~ −0.5 eV and ~ −0.7 eV. Subsequently, the activation energy of the first dehydrogenation is small and less than 0.20 eV for all the studied sites. However, this reaction is more probable on the stepped surfaces, and also on the (110); being this CeO_2 surface reactivity similar to the one found for water dissociation. The reverse reaction is unlikely both on (110) and on the stepped (331) surfaces.

The first dehydrogenation step could occur by breaking the C—H methyl bond or by breaking the O—H alcoholic bond. We found that the last reaction is much more favourable than the former.

From an energetic point of view the dehydrogenation from methoxy to formaldehyde would seem to be the rate-determining step on the stepped surface. However, the formaldehyde decomposition to formyl species on $CeO_2(111)$ have an important energetic cost and this reaction could occur only on stepped surfaces.

All the TS and the FS relative energies for (111) are higher than the ones for (331), being the stepped surface the most reactive for the decomposition of methanol.

Acknowledgements

This research was carried out for the financial support of CONICET (PIP 112-2010100949), ANPCYT (PICT 2010 – N° 0830) and Universidad Nacional del Sur (PGI – UNS N° 24/F051).

References

[1] M. Nielsen, E. Alberico, W. Baumann, H.-J. Drexler, H. Junge, S. Gladiali, M. Beller, Low-temperature aqueous-phase methanol dehydrogenation to hydrogen and carbon dioxide, Nature 495 (2013) 85–89.
[2] A. Trovarelli, Catalytic properties of ceria and CeO_2- containing materials, Catal. Rev. 38 (1996) 439–520.
[3] Catalysis by Ceria and Related Materials, in: A. Trovarelli (Ed.), Imperial College Press, London, 2002.
[4] M.S. Dresselhaus, I.L. Thomas, Alternative energy technologies, Nature 414 (2001) 332–337.

[5] V. Esposito, E. Traversa, Design of electroceramics for solid oxides fuel cell applications: playing with ceria, J. Am. Ceram. Soc. 91 (2008) 1037–1051.
[6] J.C. Brown, E. Gulari, Hydrogen production from methanol decomposition over Pt/Al_2O_3 and ceria promoted Pt/Al_2O_3 catalysts, Cat. Commun. 5 (2004) 431–436.
[7] S. Imamura, T. Higashihara, Y. Saito, H. Aritani, H. Kanai, Y. Matsumura, N. Tsuda, Decomposition of methanol on Pt-loaded ceria, Cat. Today 50 (1999) 369–380.
[8] J. Zhou, D.R. Mullins, Rh-promoted methanol decomposition on cerium oxide thin films, J. Phys. Chem. B. 110 (32) (2006) 15994–16002.
[9] D.R. Mullins, M.D. Robbins, J. Zhou, Adsorption and reaction of methanol on thin-film cerium oxide, Surf. Sci. 600 (2006) 1547–1558.
[10] D.R. Mullins, S.D. Senanayake, T.-L. Chen, Adsorption and reaction of C_1-C_3 alcohols over $CeO_X(111)$ thin films, J. Phys. Chem. C 114 (2010) 17112–17119.
[11] A. Siokou, R.M. Nix, Interaction of methanol with well-defined ceria surfaces: reflection/absorption infrared spectroscopy, X-ray photoelectron spectroscopy, and temperature-programmed desorption study, J. Phys. Chem. B 103 (33) (1999) 6984–6997.
[12] Z. Wu, M. Li, D.R. Mullins, S.H. Overbury, Probing the surface sites of CeO_2 nanocrystals with well-defined surface planes via methanol adsorption and desorption, ACS Catal. 2 (2012) 2224–2234.
[13] D. Mei, N. Aaron Deskins, Michel Dupuis, Qingfeng Ge, Methanol adsorption on the clean $CeO_2(111)$ surface: a density functional theory study, J. Phys. Chem. C 111 (2007) 10514–10522.
[14] D. Mei, N. Aaron Deskins, Michel Dupuis, Qingfeng Ge, Density functional theory study of methanol decomposition on the $CeO_2(110)$ surface, J. Phys. Chem. C 112 (2008) 4257–4266.
[15] A. Beste, D.R. Mullins, S.H. Overbury, R.J. Harrison, Adsorption and dissociation of methanol on the fully oxidized and partially reduced (111) cerium oxide surface: dependence on the configuration of the cerium 4f electrons, Surf. Sci. 602 (2008) 162–175.
[16] A. Beste, S.H. Overbury, Hydrogen and methoxy coadsorption in the computation of the catalytic conversion of methanol on the ceria (111) surface, Surf. Sci. 648 (2016) 242–249.
[17] J.E. Sutton, S.H. Overbury, A. Beste, Coadsorbed species explain the mechanism of methanol temperature-programmed desorption on $CeO_2(111)$, J. Phys. Chem. C 120 (2016) 7241–7247.
[18] T. Kropp, J. Paier, J. Sauer, Support effect in oxide catalysis: methanol oxidation on vanadia/ceria, J. Am. Chem. Soc. 136 (2014) 14616–14625.
[19] T. Kropp, J. Paier, Reactions of methanol with pristine and defective ceria (111) surfaces: a comparison of density functionals, J. Phys. Chem. C 118 (2014) 23690–23700.
[20] T. Kropp, J. Paier, Activity versus selectivity of the methanol oxidation at ceria surfaces: a comparative first-principles study, J. Phys. Chem. C 119 (2015) 23021–23031.
[21] M. Capdevila-Cortada, M. García-Melchor, N. López, Unraveling the structure sensitivity in methanol conversion on CeO_2: a DFT + U study, J. Catal. 327 (2015) 58–64.
[22] N. Kumari, N. Sinha, M.A. Haider, S. Basu, CO_2 reduction to methanol on CeO_2 (110) surface: a density functional theory study, Electrochim. Acta 177 (2015) 21–29.
[23] N. Kumari, M.A. Haider, M. Agarwal, N. Sinha, S. Basu, Role of reduced $CeO_2(110)$ surface for CO_2 reduction to CO and methanol, J. Phys. Chem. C 120 (2016) 16626–16635.
[24] Z. Cheng, B.J. Sherman, C.S. Lo, Carbon dioxide activation and dissociation on ceria (110): a density functional theory study, J. Chem. Phys. 138 (014702) (2013) 1–12.
[25] Z. Cheng, C.S. Lo, Mechanistic and microkinetic analysis of CO_2 hydrogenation on ceria, Phys. Chem. Chem. Phys. 18 (2016) 7987–7996.
[26] M.M. Branda, R.M. Ferullo, M. Causá, F. Illas, Relative stabilities of low index and stepped CeO_2 surfaces from hybrid and GGA + *U* implementations of density functional theory, J. Phys. Chem. C 115 (2011) 3716–3721.
[27] J.P. Perdew, J.A. Chevary, S.H. Vosko, K.A. Jackson, M.R. Pederson, D.J. Singh, C. Fiolhais, Atoms, molecules, solids, and surfaces: applications of the generalized gradient approximation for exchange and correlation, Phys. Rev. B 46 (1992) 6671.
[28] J.P. Perdew, J.A. Chevary, S.H. Vosko, K.A. Jackson, M.R. Pederson, D.J. Singh, C. Fiolhais, Erratum: atoms, molecules, solids, and surfaces: applications of the generalized gradient approximation for exchange and correlation, Phys. Rev. B 48 (1993) 4978.
[29] S.L. Dudarev, G.A. Botton, S.Y. Savrasov, C.J. Humphreys, A.P. Sutton, Electron-energy-loss spectra and the structural stability of nickel oxide: an LSDA + U study, Phys. Rev. B 57 (1998) 1505–1509.
[30] C. Loschen, J. Carrasco, K.M. Neyman, F. Illas, First-principles LDA + u and GGA + u study of cerium oxides: dependence on the effective U parameter, Phys. Rev. B 75 (035115) (2007) 1–8.
[31] A. Migani, G.N. Vayssilov, S.T. Bromley, F. Illas, K.M. Neyman, Greatly facilitated oxygen vacancy formation in ceria nanocrystallites, Chem. Commun. 46 (2010) 5936–5938.
[32] A. Migani, G.N. Vayssilov, S.T. Bromley, F. Illas, K.M. Neyman, Dramatic reduction of the oxygen vacancy formation energy in ceria particles: a possible key to their remarkable reactivity at the nanoscale, J. Mater. Chem. 20 (2010) 10535–10546.
[33] C. Loschen, A. Migani, S.T. Bromley, F. Illas, K.M. Neyman, Density functional studies of model cerium oxide nanoparticles, Phys. Chem. Chem. Phys. 10 (2008) 5730–5738.
[34] A. Migani, C. Loschen, F. Illas, K.M. Neyman, Towards size-converged properties of model ceria nanoparticles: monitoring by adsorbed CO using DFT + U approach, Chem. Phys. Lett. 465 (2008) 106–109.
[35] A. Migani, K.M. Neyman, F. Illas, S.T. Bromley, Exploring Ce^{3+}/Ce^{4+} cation ordering in reduced ceria nanoparticles using interionic-potential and density-functional calculations, J. Chem. Phys. 131 (64701) (2009) 1–7.
[36] P.E. Blöchl, Projector augmented-wave method, Phys. Rev. B 50 (1994) 17953–17979.
[37] H.J. Monkhorst, J.D. Pack, Special points for Brillouin-zone integrations, Phys. Rev. B: Solid State 13 (1976) 5188–5192.
[38] M. Methfessel, A.T. Paxton, High-precision sampling for Brillouin-zone integration in metals, Phys. Rev. B 40 (1989) 3616–3621.
[39] S. Grimme, Semiempirical GGA-type density functional constructed with a long-range dispersion correction, J. Comput. Chem. 27 (2006) 1787–1799.
[40] J.P. Perdew, K. Burke, M. Ernzerhof, Generalized gradient approximation made simple, Phys. Rev. Lett. 77 (1996) 3865–3868.
[41] H. Jonsson, G. Mills, K.W. Jacobsen, Nudged Elastic Band Method for Finding Minimum Energy Paths of Transitions, in: B.J. Berne, G. Ciccotti, D.F. Coker (Eds.), World Scientific, Singapore, 1998, pp. 385–404, ISBN: 978-981-02-3498-0.
[42] G. Kresse, J. Furthmuller, Efficient iterative schemes for ab initio total-energy calculations using a plane-wave basis set, Phys. Rev. B: Condens. Matter Mater. Phys. 54 (1996) 11169–11186.
[43] G. Kresse, J. Hafner, Ab initio molecular dynamics for liquid metals, Phys. Rev. B: Condens. Matter Mater. Phys. 47 (1993) 558–561.
[44] J. Duclos, Y.K. Vohra, A.L. Ruoff, A. Jayaraman, G.P. Espinosa, High-pressure x-ray diffraction study of CeO_2 to 70 GPa and pressure-induced phase transformation from the fluorite structure, Phys. Rev. B 38 (1988) 7755–7758.
[45] S.A. Fuente, M.M. Branda, F. Illas, Role of step sites on water dissociation on stoichiometric ceria surfaces, Theor. Chem. Acc. 131 (2012) 1190–1196.